The HKU Scholars Hub   The University of Hong Kong   香港大學學術庫

Title	**Ultrafast and versatile spectroscopy by temporal Fourier transform**
Author(s)	**ZHANG, C; WEI, X; Marhic, ME; Wong, KKY**
Citation	**Scientific Reports, 2014, v. 4, p. 5351**
Issued Date	**2014**
URL	**http://hdl.handle.net/10722/202827**
Rights	**Creative Commons: Attribution 3.0 Hong Kong License**

Correspondence and requests for materials should be addressed to K.K.Y.W. (kywong@eee.hku.hk)

Ultrafast and versatile spectroscopy by temporal Fourier transform

Chi Zhang[1], Xiaoming Wei[1], Michel E. Marhic[2] & Kenneth K. Y. Wong[1]

[1]Photonic Systems Research Laboratory, Department of Electrical and Electronic Engineering, The University of Hong Kong, Pokfulam Road, Hong Kong, [2]College of Engineering, Swansea University, Singleton Park, Wales SA2 8PP, UK.

One of the most remarkable and useful properties of a spatially converging lens system is its inherent ability to perform the Fourier transform; the same applies for the time-lens system. At the back focal plane of the time-lens, the spectral information can be instantaneously obtained in the time axis. By implementing temporal Fourier transform for spectroscopy applications, this time-lens-based architecture can provide orders of magnitude improvement over the state-of-art spatial-dispersion-based spectroscopy in terms of the frame rate. On the other hand, in addition to the single-lens structure, the multi-lens structures (e.g. telescope or wide-angle scope) will provide very versatile operating conditions. Leveraging the merit of instantaneous response, as well as the flexible lens structure, here we present a 100-MHz frame rate spectroscopy system – the parametric spectro-temporal analyzer (PASTA), which achieves 17 times zoom in/out ratio for different observation ranges.

The optical spectrum acts as an information carrier of many dynamic chemical or physical phenomena, and ultrafast spectroscopy is able to directly observe the peptide conformational dynamics[1]. Moreover, examples of bio-imaging systems that rely on spectroscopy in the final end are coherent anti-Stokes Raman scattering (CARS) microscopy[2] and serial time-encoded amplified microscopy (STEAM)[3]. Therefore, how to capture the spectral information in an accurate and ultrafast manner is an essential problem, especially for some ultrafast or non-repetitive phenomena, such as for bio-imaging[4] or gas absorption[5] applications. One recent example about fluorescence imaging was the introduction of some nano-particles, which showed significant improvement on distinguishing against the autofluorescent background of the surrounding tissue[6]. However, in order to rapidly screen the attachment of the large number of particles, ultrafast spectroscopy is still required. The most conventional spectroscopic technique is based on the mechanical rotation of spatially dispersive components (e.g. diffraction grating); this achieves great spectral accuracy but limited operating speed[7]. More recently, another method called amplified dispersive Fourier transformation (ADFT) introduced the concept of single-shot and single-pixel data acquisition by dispersively stretching the spectrum of short pulses in the time domain[8,9]. Although ADFT can be operated very fast, the restricted input pulse conditions and the relatively low detection sensitivity limit its operation range.

The accuracy of a spectroscopy system is fundamentally limited by Fourier transform theory; it can be defined by the effective time-bandwidth product (eTBP). Here, the time corresponds to the frame period T, and the bandwidth corresponds to the finest frequency resolution Δv. It is necessary for the frequency resolution Δv to be of the order of the width of the finest features of the spectrum. From Fourier transform theory we know that the scale of such features is of the order of $1/T$. Hence a well-optimized system of this type should be such that the eTBP $\Delta v \times T \sim 1$. This criterion can be used to quantify how close to the limit a particular system operates. It can also be used for comparing different systems of this type, and by contrast previous systems such as OSA and ADFT only have eTBP of the order of 5×10^8 and 200, respectively, much further away from this limit. For the precise definition of the eTBP, see the Methods.

Recently we proposed a new spectroscopy scheme called parametric spectro-temporal analyzer (PASTA), based on the time-lens focusing mechanism[10,11]. Comparing with the direct dispersive stretching of the ADFT, PASTA incorporates a converging time-lens in front of the dispersion. This greatly relaxes the input limitations: the input signals can range from short pulses ($\sim$ps or $\sim$fs) to arbitrary waveforms across the observation window (see Supplementary Information). Since the same wavelength is focused after the focal group-dispersion delay (GDD), the detection sensitivity is greatly enhanced. The first demonstrated single-lens PASTA achieved 0.03-nm spectral resolution over a 5-nm wavelength range, with −32-dBm detection sensitivity at 100-MHz frame rate, with the eTBP down to 25[10,11]. However, this configuration is not flexible in terms of the observation range, since
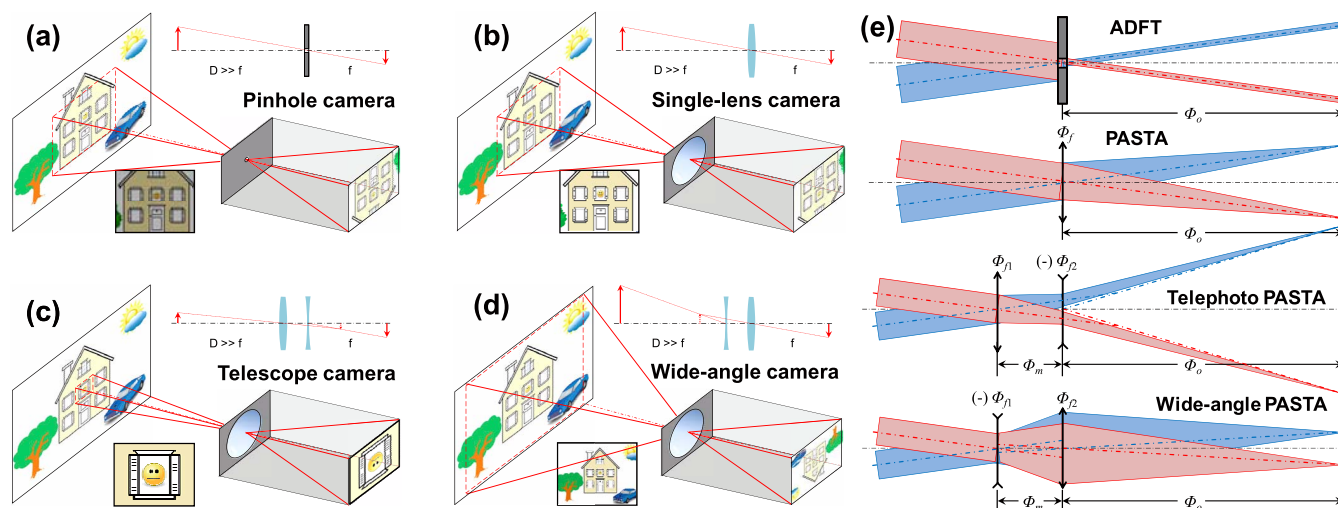
Figure 1 | Analogy between four spatial imaging systems and the ray diagrams of their temporal counterparts. (a), Pinhole camera. (b), Single-lens camera. (c), Telescope camera. (d), Wide-angle camera. (e), Temporal ray diagram shows that the operating principles of the time-lens mechanisms are analogous to the space-lens counterparts. These four time-lens mechanisms share the same output dispersion (Φ_o). (This figure was generated by C. Z.).

the wavelength-to-time mapping relation is completely determined by the dispersion value, which is not easy to adjust for a given spool of fiber.

A more comprehensive tool is essential in designing ultrafast spectroscopic systems, besides incorporating the observation range of ADFT and PASTA. It is preferable to develop additional mechanisms, so as to obtain a sharper spectral resolution or a wider wavelength range in various applications. In this article, we propose a unified approach for ultrafast spectroscopy in the time domain, by analogy with some spatial imaging systems. By pursuing this unified approach, we not only obtain a comprehensive understanding of ADFT and PASTA, but we also incorporate the concept of telescope and wide-angle scope into the PASTA system. As a result, while keeping the same output dispersion, we are able to achieve a flexible observation range by leveraging the spectrum zoom-in feature of a pair of time-lenses configured as a temporal telescope[12]. Applying this idea to the single-lens PASTA, we successfully improve the resolution from 0.02 nm to 0.005 nm, though the observation range is narrowed as well. As a result, we have achieved the record eTBP $\sim$ 6.25, which is over 8 orders of magnitude improvement over conventional laboratory spectroscopy – optical spectrum analyzer (OSA, e.g. Yokogawa AQ6370C[13]) eTBP $\sim 5 \times 10^8$, and of the order of the eTBP limit. Alternatively, when we configure this pair of time-lenses as a wide-angle scope, which can zoom out the spectrum under test, the wide-angle PASTA expands the observation range from 5 nm to 10 nm. In all these cases, we verify that the PASTA is particularly suitable for observing non-repetitive spectra or even unstable spectra by its dynamic process, without the need for any post-processing or synchronization. This unified approach opens a new horizon for ultrafast spectroscopy, as well as ultrafast bio-imaging applications.

Results

Implementation of temporal telescope or wide-angle scope by space-time duality. The discovery of the space-time duality between two apparently disparate physical phenomena, paraxial diffraction and narrow-band dispersion, helps to shed new light and understanding on both of them[14]. Therefore, some spatial-domain mechanisms, such as magnification/demagnification in imaging and Fourier transform, have also been demonstrated in the temporal domain[15–17]. To enlarge the spectral observation range (zoom in/out) in the temporal domain, we may also resort to its spatial counterpart, the camera system as shown in Fig. 1. It illustrates four spatial imaging systems: the pinhole camera, the

single-lens camera, the telescope camera, and the wide-angle camera. The first two configurations are analogous to the ADFT and the single-lens PASTA. In addition, the flexibility problem of the single-lens camera can be solved by a pair of lenses in the telescope/wide-angle camera as shown in Fig. 1(c) and (d), which zooms in/out to achieve different fields of view (FOV). Similarly, if we can implement a pair of time-lenses as in the telescope/wide-angle camera, the observation range of the PASTA will be greatly enhanced as shown in Fig. 1(e).

We will start with the comparison of the pinhole camera and the single-lens camera (Fig. 1(a) and (b)), which are analogous to the ADFT and the single-lens PASTA in the temporal domain (the upper two panels in Fig. 1(e), respectively). In the case of the pinhole camera, the smaller the hole, the sharper the image one can obtain (until diffraction becomes important), but at the expense of the brightness of the projected image (typical exposures range from 5 seconds to several hours)[18]. It can be observed from Fig. 1(e) that the pinhole size is analogous to the input pulsewidth of the ADFT; hence the shorter the pulsewidth, the sharper the spectral resolution one can obtain, but at the expense of the detection sensitivity, since only a small portion of the incoming light can pass through the limited time slot[9]. As the concept of focus does not apply to the pinhole camera, the distance from the pinhole to the sensor can be flexible; in the case of the ADFT mechanism, we can adjust the output dispersion to achieve different resolutions[19]. Furthermore, the introduction of the imaging lens in the camera greatly improves the resolution and the sensitivity over the pinhole camera, though both achieve the same FOV for the same image distance. As a result, the pinhole camera is mainly used for some artistic applications nowadays[18]. If the camera is focused on objects at infinity, the distance from the exit pupil to the sensor is equal to the focal length. It is the same concept for the single-lens PASTA configuration (the second panel in Fig. 1(e)): as long as the output GDD is equal to the focal GDD ($\Phi_o = \Phi_f$), better detection sensitivity and resolution can be achieved, because the larger pupil size (or temporal observation window) captures most of the incoming light[10,11].

With the advancing development of the camera system, the concept of the telephoto lens (single lens with long focal length) or wide-angle lens have greatly enhanced the observation capability of the camera, and some commercial single-lens reflex (SLR) cameras have achieved optical zoom in/out ratio over 16 (Nikon AF-S DX Nikkor 18–300 mm f/3.5–5.6 G)[20]. However, there are some problems for this adjustable single-lens system: (i) the telephoto lens requires a

longer distance from the lens to the sensor; (ii) the wide-angle lens requires a larger temporal aperture. To reduce the physical dimension of the whole system, a pair of lenses with the function of the telescope or wide-angle scope is added in front of a standard single-lens camera, and this method can achieve the same functionality as the corresponding telephoto or wide-angle lens camera. According to the space-time duality, one can map this spatial mechanism into the temporal domain, as illustrated by the optical paths of the temporal ray diagrams in Fig. 1(e). Here the eyepiece and the single camera lens are combined together as the second lens, since there is no distance between them[21]. The first lens (objective lens) images the infinitely distant objects close to the focal length of the eyepiece, and the second lens (combining the eyepiece and the original single-lens) further images it onto the sensor. In the temporal domain, this two-lens configuration largely reduces the dispersion, compared with the single telephoto time-lens (essential when large dispersion is involved as shown in the Methods). Keeping the same output dispersion, we can design the whole set of PASTA configurations with a specified zoom in/out ratio.

Detailed experimental setup for the telescope/wide-angle PASTA. There are two time-lenses involved in the telescope/wide-angle PASTA, and they are implemented by two stages of four-wave mixing (FWM). A pulsed source (2-ps pulsewidth) passing through different pump dispersions provides the swept pumps for two FWMs[22,23]. It is noted that every stage of FWM also acts as a spectral mirror (or phase conjugator)[24]; therefore, it is required to have an even number of stages to compensate this effect. This explains why in the single-lens PASTA configuration, the single time-lens was also implemented by two stages of FWM: the

second-stage FWM pumped by a CW source ($\Phi_{p2} = +\infty$ ps²) only acted as a spectral mirror[10]. Since there is no dispersion between these two FWMs, the mid-span dispersion $\Phi_m = 0$ ps², as shown in Fig. 2(a) and Table 1. In the case of the telescope/wide-angle PASTA, as in the space-lens, the distance between the two lenses is critical to control the divergence of the light beam; the mid-span dispersion (Φ_m) between the two time-lenses is important to adjust the wavelength-to-time ratio.

The overall setup can be simply viewed as two time-lenses inserted with a mid-span dispersion (Φ_m) and followed by the output dispersion (Φ_o), as shown in Fig. 2(a). It is noticed that the time-lens and the dispersion processes change the chirp rate (the slope of the wavelength-to-time ratio) in a different manner, as shown in Fig. 2(b) and (c). During the time-lens process, the wavelength separation is maintained but the temporal spacing is adjusted; while for the mid-span or output dispersions, the temporal spacing is maintained but the wavelength separation is adjusted[25]. For example, the input of the telescope PASTA (Fig. 2(b)) starts from two close CW sources (parallel with small spacing). In time-lens 1, a small chirp rate is introduced by the large negative pump dispersion (Φ_{p1} by dispersion compensating fiber (DCF)), while the wavelength separation remains small. Then the positive mid-span dispersion (Φ_m by single-mode fiber (SMF)) increases the chirp rate with fixed temporal spacing; therefore the wavelength separation is enlarged. In time-lens 2, the eyepiece (dash-dotted line in Fig. 2(b)) will convert the chirp rate into zero (parallel line). Since the wavelength separation is maintained and the temporal spacing is broadened, it realizes the function of telescope (spectral zoom in)[12]. Considering the eyepiece and the PASTA lens are combined together as a single time-lens 2, namely by introducing a slightly larger pump dispersion (Φ_{p2} by DCF, the solid line in

(a) Setup

Swept-Pump 1   Swept-Pump 2

EDFA   Filter   Filter   EDFA
Φ_{p1} Pulse Source Φ_{p2}

FWM1   Filter   EDFA   FWM2   Filter
Φ_{f1} Φ_m Φ_{f2} Φ_o

Input   Output

Time-lens 1   Time-lens 2

(b) Telescope PASTA

Φ_m SMF Φ_{p2} Φ_o DCF   Output Δt

Φ_{p1} Input $\Delta\lambda$

Time-lens 1   Time-lens 2

(c) Wide-angle PASTA

Φ_m DCF Φ_{p2} Φ_o DCF   Output Δt

Φ_{p1} Input $\Delta\lambda$
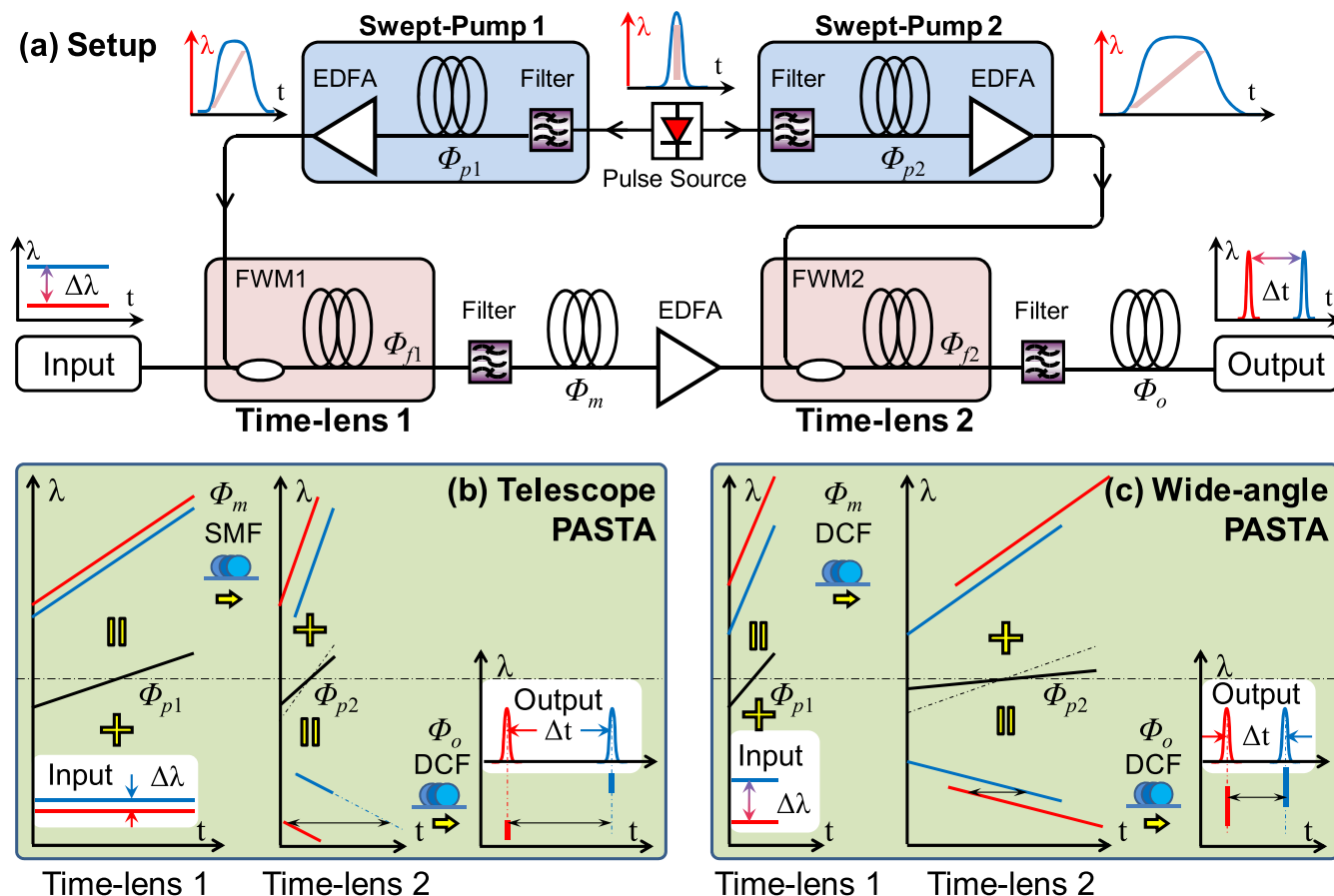
Time-lens 1   Time-lens 2

Figure 2 | Design and implementation of the telescope/wide-angle PASTA. (a), Detailed experimental setup. Two time-lenses are achieved by a FWM-based parametric mixer, and the two swept pumps are derived from the same pulsed source, passing through different dispersive fibers. (b) & (c), The signal wavelength-to-time ratio changes step by step through the telescope/wide-angle PASTA process.

Table 1 | Detailed dispersion configuration of the single-lens PASTA and the telescope/wide-angle PASTA (including the fiber length and the GDD)

	Single-lens PASTA		Telescope PASTA		Wide-angle PASTA	
	Fiber	GDD	Fiber	GDD	Fiber	GDD
Pump 1 (Φ_{p1})	32.6-km DCF 13.1-km SMF	4900 ps^2	12.4-km DCF	1990 ps^2	6.93-km DCF	1116 ps^2
Mid-span (Φ_m)	None	0 ps^2	37.8-km SMF	−892 ps^2	2.65-km DCF	456 ps^2
Pump 2 (Φ_{p2})	CW Source	+∞ ps^2	1.33-km DCF	214 ps^2	22.0-km DCF 4.15-km SMF	3460 ps^2
Output (Φ_o)	16.3-km DCF	2450 ps^2	16.3-km DCF	2450 ps^2	16.3-km DCF	2450 ps^2

Fig. 2(b)). Therefore, the wavelength-to-time ratio is reversed after time-lens 2, and can be compressed by the negative output dispersion (Φ_o by DCF), which keeps increasing the chirp rate. To sum up, the telescope PASTA achieves high spectral resolution by increasing the temporal spacing; the opposite is true for the wide-angle configuration, which achieves a wide wavelength range by decreasing the temporal spacing, as shown in Fig. 2(c).

For either telescope or wide-angle PASTA, four spools of dispersive fibers are involved, including two pump dispersions (Φ_{p1} and Φ_{p2}), the mid-span dispersion (Φ_m), and the output dispersion (Φ_o). The detailed dispersion configurations (including the fiber length and the GDD) of the telescope/wide-angle PASTA are shown in Table 1. The time-lens focusing mechanism requires that these four GDD values satisfy certain relations, and the zoom in/out ratio is also determined by these dispersions (for a quantitative description of the GDD relation, see the Methods).

Stationary performance. Although all these PASTA configurations are capable of capturing dynamic or stationary spectrum evolution with 100-MHz frame rate[10], stationary CW sources are easier to be quantitatively characterized than single-shot counterparts. The time-lens focusing mechanism can focus the CW sources into temporal pulses; however, due to the limited detection bandwidth (16 GHz), the shortest detectable electrical pulsewidth is 40 ps. Noted that although there are some timing jitters, the relative accuracy will not be degraded, since the whole frame is shifted synchronously within a single-shot spectrum. In other words, the timing jitter only offsets the absolute wavelength (which can be calibrated later), but not the relative wavelength position.

The stationary performance of the PASTA configurations measured with the CW source is shown in Table 2 and Fig. 3. First, the telescope PASTA has much larger timing jitter (400 ps), as shown in Fig. 3(a), because the timing jitter of the swept-pump was enlarged during the spectral zoom-in process. Second, the ideal pulse amplitude reflects the intensity of the signal under test, but it is degraded by the two-stage FWM process, especially the intensity fluctuation of the swept pump. It is observed from Fig. 3(c) and (e) that the intensity fluctuation is around 20% of the peak power. The telescope/wide-angle PASTA shows 8-dB better detection sensitivity (−40 dBm) than that of the single-lens PASTA (−32 dBm). This is because in the single-lens PASTA, the second stage FWM was pumped by a CW source, and the lower stimulated Brillouin scattering (SBS) threshold limited its conversion efficiency[26].

To observe the multi-wavelength response of these PASTA configurations, under different zoom in/out ratio, four approximately equally-spaced CW sources were launched into the PASTAs with different separations. First, in the case of the telescope PASTA, four CW sources were roughly spaced by 0.1 nm (black solid line in Fig. 3(b)), and it achieved much sharper spectral resolution (0.005 nm) than a conventional OSA (Agilent 86142B, 0.06 nm, the red dash-dotted line)[29]. Since the observation range of the single-lens PASTA was 5 nm, the wavelength spacing was increased to 1 nm as shown in Fig. 3(d). Similarly, the wavelength spacing was increased to 1.9 nm for the wide-angle PASTA, as shown in Fig. 3(f). These two configurations also show better resolution compared to

the OSA. Moreover, the single-lens PASTA has a uniform intensity envelope (Fig. 3(d)), compared to the telescope/wide-angle PASTA. The intensity envelope over the observation wavelength range was determined by the temporal aperture of the second-stage time-lens (or FWM). For the single-lens PASTA, the second-stage FWM was pumped by a CW source, so the temporal aperture covered the whole period, and achieved uniform conversion efficiency[10,26]. On the contrary, as in the case of telescope PASTA, the stretched pump pulse-width was 500 ps (temporal aperture), and the wavelength detuned from the central wavelength will have a low conversion efficiency. Similarly for the wide-angle PASTA case (bottom of the Fig. 1(e)), where the first diverging time-lens expands the beam size, and part of energy will not be covered by the limited temporal aperture (2 ns) of the second time-lens.

Besides using CW sources to quantify the performance of the PASTA system, we can also observe a variety of pulse sources. For some low repetition rate short pulses (<1 GHz), the ADFT configuration is still preferable, owing to its ease of implementation; in the PASTA system, some intensity noise is introduced through the two-stage FWM (see Supplementary Information), and the energy converging to enhance the sensitivity no longer exists. However, beyond the ADFT observation window, PASTA can observe the aforementioned CW source, as well as higher repetition rate pulse trains (>1 GHz, e.g. 10-GHz communication source), or some non-periodic signals (e.g. a pseudorandom binary sequence (PRBS) data sequence). These results are shown in Fig. 4, where we used a 10-GHz communication pulse source (*Alnair*, MLLD-100). Figure 4(a) is its spectrum obtained by the conventional OSA, while Fig. 4(b) is its real-time spectrum obtained by our 100-MHz single-lens PASTA system, which shows better resolution over the OSA system. If we further add a 2^7 PRBS data sequence to modulate this pulse train, its spectrum obtained by the PASTA system is shown as Fig. 4(c): the overall intensity drops, while the 5-GHz sub-frequencies rise.

Discussion

In this article, we present, for the first time, single-shot spectrum measurements of dynamic spectra using a pair of time-lenses. We achieved 17 times optical zoom in/out ratio with frame rate of 100 MHz. These PASTA configurations greatly relax the input conditions of the signal under test, which can be an arbitrary waveform across the observation window and without the need for any post-processing and synchronization. By overcoming the limitation of the SBS threshold in the single-lens PASTA, the telescope/wide-angle PASTA achieves detection sensitivity as low as −40 dBm, as well as over 1000 of dynamic range. The functionality of the telescope/wide-angle PASTA was tested here with stationary CW sources, and the ultrafast dynamic spectrum acquisition was demonstrated based on the single-lens PASTA. The maximum observation span of 256 μs was not fundamental but simply limited by the available memory depth of 20.5 mega-points at sampling rate of 80-GSa/s.

However, it should be noted that the currently demonstrated observation wavelength bandwidth (5–10 nm) of the PASTA restricts its applications. According to the aforementioned discussion, the observation bandwidth is primarily limited by the wave-

Table 2 | Performance of different PASTA configurations

Specifications	FROG [27] (Mesa Photonics)	OSA [13] AQ6370C (Yokogawa)	BOSA [28] (Aragon Photonics)	ADFT [8]	PASTA		
					Wide-angle	Single-lens	Telescope
Resolution (nm)	0.2	0.02	8×10^{-5}	0.04	0.047	0.02	0.005
Wavelength range (nm)	100–600	100	37	$10^{(4)}$	10	5	0.56
Frame rate	2 Hz	5 Hz	1 Hz	25 MHz		100 MHz	
Input condition	Short pulse	Any	Any	Short pulse		Any	
Observation span	30 ps	Any	Any	~20 ms		~20 ms	
Time/λ (ns/nm)					$-1.067^{(1)}$	$-1.97^{(1)}$	$-17.7^{(1)}$
Zoom in/out ratio					0.54	1	9
Sensitivity (dBm)	$>30^{(3)}$	-60	-70	$>30^{(3)}$	$-40^{(2)}$	$-32^{(2)}$	$-40^{(2)}$
eTBP	1.25×10^{10}	5×10^{8}	1×10^{7}	200	59	25	6.25

[1]This negative sign is due to the normal output dispersion, which makes the initial time corresponds to the longer wavelength.
[2]Single-lens PASTA sensitivity is worse than for the telescope/wide-angle configuration, because in the second-stage FWM, the SBS threshold limited the CW pump power.
[3]Since the FROG and the ADFT systems primarily measure the short pulse, here the sensitivity refers to the peak power of the pulse.
[4]Here the wavelength range is only for this specified application, the DFT process can be operated on much wider wavelength range, e.g. over 100 nm.

length conversion bandwidth of the FWM, which is affected by the dispersion-related phase-matching condition. In our PASTA prototype, a highly-nonlinear dispersion-shifted fiber (HNL-DSF) was employed as the nonlinear medium. The higher-order dispersion coefficients ($\beta_2 = 5.78 \times 10^{-2}$ ps²/km and $\beta_3 = -1.41 \times 10^{-4}$ ps³/km) limited the single-side conversion bandwidth to be 10 nm[26]. Recent development of dispersion-engineered nonlinear media, especially the silicon nanowaveguide, helped to achieve 300-nm wavelength conversion bandwidth on the single-side of FWM[30]. Therefore, implementing the PASTA system in such kind of device would make it not only more compact, but also promising for achieving over 100-nm observation bandwidth (see Supplementary Information). It is noted that, larger bandwidth resulted in lower repetition rate, to avoid any overlapping between the neighboring period, e.g. 100-nm bandwidth requires a 200-ns time window. In addition to enlarging the existing bandwidth, it is also possible to develop a PASTA system centered in a different wavelength region. A benefit from the two-stage FWM structure, which compensates the accompanying phase conjugation, is that it guarantees that the pump dispersion and the output dispersion are of the same type (normal or anomalous). This feature is essential for some wavelength bands, where it can only provide large values of normal dispersion (e.g. at 1 μm and visible range). Consequently, we believe that the channelized configuration (PASTAs covering different wavelength bands operating simultaneously) will further enhance its spectral resolving ability.

On the other hand, these PASTA prototypes have not been optimized for detection sensitivity and noise figure performance[31]. Figure 5 illustrates the basic structure of the single-lens PASTA system: two cascaded FWM-based wavelength conversion stages, as well as a booster amplifier in between. According to the aforementioned measurement, the signal sensitivity ranged from −32 dBm to 0 dBm, which were treated as the references for our analysis. The variations of the signal power between these boundaries are shown in Fig. 5(a). Here, we employed a 24-GHz PIN photodetector (Agilent, 83440D), with detection sensitivity down to −20 dBm. To further enhance the detection sensitivity, another booster amplifier was inserted in the front, as the dashed triangle shown in Fig. 5. It is noticed that there is a 20-dB improvement for the signal-to-noise ratio (SNR) at the output dispersion; since during the temporal converging process, the signal distributed across the 10-ns period was accumulated into the 50-ps pulsewidth. Therefore, the temporal intensity was enhanced by 20 dB. On the other hand, the distribution of the noise was unchanged such that the signal SNR was improved by 20 dB. With more accurate noise figure control, we believe that the PASTA system can achieve detection sensitivity as low as −50 dBm, which corresponds to 781 photons within the 10-ns time period.

As an overview of ultrafast spectrum measurements, the whole category of the PASTA system has enriched the capability of our tool box. The advent of the ADFT technology started the era of the temporal spectrum analyzer, and it is easy to implement with stable results, however it is only capable of measuring some low-repetition-rate short pulses (see Supplementary Information). To enlarge the temporal observation window, a time-lens was first included in the single-lens PATSA system. Although it introduces intensity noise as well, for the first time the PASTA system makes long pulse measurements possible as an ultrafast temporal spectrum analyzer: it can characterize CW sources as well as some non-periodic waveforms. To further enhance the wavelength observation range of PASTA, a two-time-lens structure was introduced here, which renders temporal spectrum measurements more versatile. Each mechanism has its optimum application range. For example, if we observe low-repetition-rate short pulses by PASTA, the time-lens will become useless (or transparent), and introduce extra intensity noise; the result will be worse than that of the simple ADFT configuration.
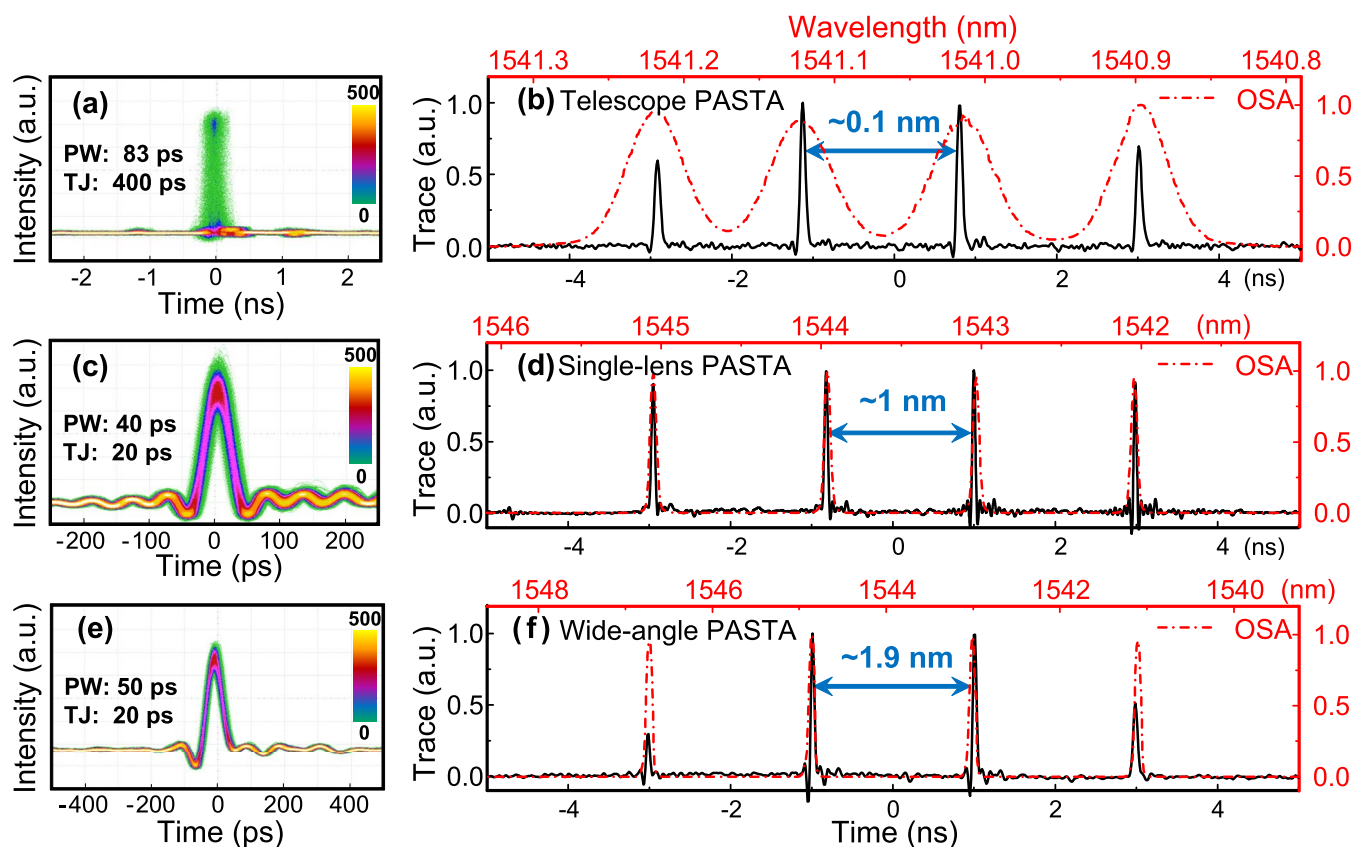
Figure 3 | Characterization of different PASTA configurations: the eye diagram with single CW source, and the single-shot trace with 4 approximately equally-spaced CW sources. (a) & (b), Telescope PASTA, 0.1 nm spacing. Large timing jitter can be removed by a suitable triggering mechanism, e.g. including a reference CW source. (c) & (d), Single-lens PASTA, 1 nm spacing. (e) & (f), Wide-angle PASTA, 1.9 nm spacing. PW: pulsewidth, TJ: Timing jitter.

To conclude, we proposed and demonstrated a unified approach for ultrafast spectroscopy in the time domain, by analogy with some spatial imaging systems. By pursuing this unified approach, we not only obtained a comprehensive understanding of ADFT and PASTA, but we also incorporated the concept of telescope and wide-angle scope into the PASTA system, which achieved larger bandwidth and better detection sensitivity than previous techniques. The analogy with the telescope and the wide-angle scope makes the PASTA system versatile for observing different wavelength ranges. Compared with previous approaches which are not time-efficient, the PASTA
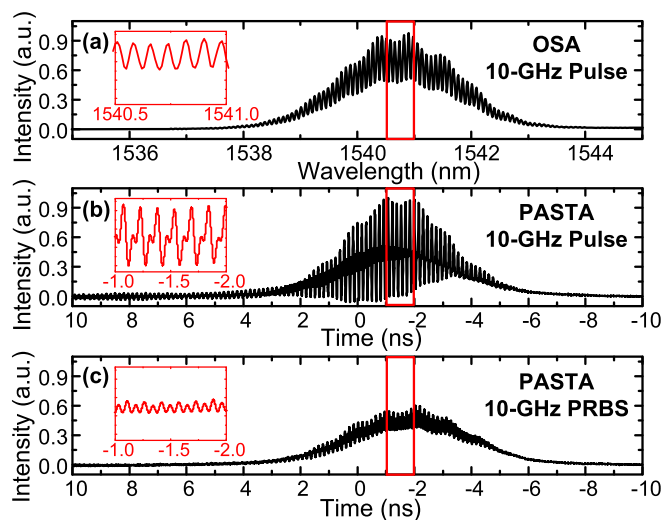
Figure 4 | Stationary performance of high repetition rate pulse train by PASTA measurement. (a), 10-GHz pulse source centered at 1540.5 nm with 2.5-ps pulsewidth. The spectrum measured by conventional OSA with resolution of 0.05 nm. (b), The same source measured by single-lens PASTA. (c), This pulse sequence modulated by 2^7 PRBS data, and measured by single-lens PASTA. Inset: zoom-in showing the detailed features of the fringes (the vertical axis scale is identical).
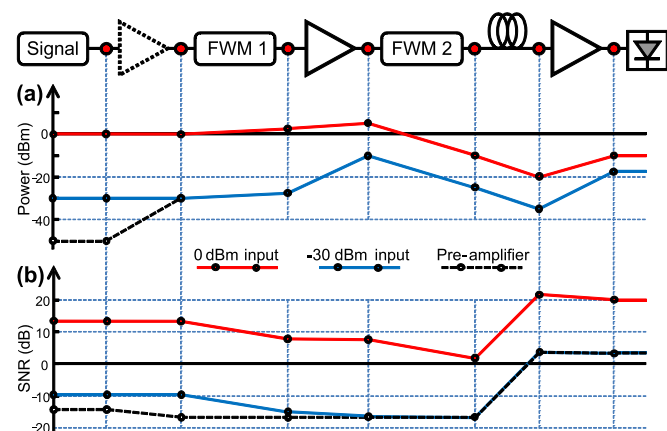

Figure 5 | Characterization of the cascaded SNR along the single-lens PASTA system. (a), Measured power budget, with the maximum and minimum input power of the dynamic range. (b), Estimated SNR variation along the channel. One more EDFA was added in front of the PASTA to further enhance the detection sensitivity, and the performance is shown by the dashed lines.

system is approaching the Fourier transform limit, with the effective time-bandwidth product down to 6.25. The whole set of PASTA configurations provides a flexible and ultrafast spectroscopy tool, and we therefore expect that this approach can be the basis for some imaging applications in areas where rapid spectral acquisition is essential.

Methods

Effective time-bandwidth product (eTBP). Some limitations apply to systems designed to acquire the optical spectra of signals. To quantify these limitations we introduce four parameters. First, in the case of systems operated with a scanning process (e.g. OSA and BOSA), or large temporal window with arbitrary signal (e.g. PASTA), we have the first two parameters: the temporal frame period T_{fr}, and the frequency resolution of the system Δv_{res}. From Fourier transform theory we know that the best resolution Δv_{res} which can be achieved is of the order of $1/T_{fr}$. Second, in the case of systems observing short-pulse signals (e.g. ADFT and FROG), we have the other two parameters: the temporal width of the signal T_p, and the corresponding size of the smallest details of the frequency spectrum Δv_p. From Fourier transform theory we have $\Delta v_p \approx 1/T_p$. Since the stretched spectrum or the operation process occupies a longer time span, the frame period T_{fr} is usually much larger than the short pulsewidth T_p. To provide a fair comparison between all these different possibilities, we should take the larger T_{fr} in the TBP calculation. Therefore, we define an effective TBP, as follows:

$$eTBP = \Delta v \cdot T = \max\{\Delta v_p, \Delta v_{res}\} \cdot \max\{T_p, T_{fr}\} \geq 1 \qquad (1)$$

Dispersion relation. Since the time-lenses are implemented by FWM, the focal GDD is half of the pump GDD, $\Phi_f = \Phi_p/2$. For the first time-lens, infinitely distant objects are imaged at the focal plane, Φ_{f1} away from the first time-lens. For the second time-lens, since the two time-lenses are spaced by Φ_m, the object GDD should be ($\Phi_{f1} + \Phi_m$), and the image GDD is equal to the output GDD Φ_o. Therefore, the temporal imaging relation is:

$$\frac{1}{\Phi_{f1} + \Phi_m} - \frac{1}{\Phi_o} = \frac{1}{\Phi_{f2}} \qquad (2)$$

Considering the zoom in/out ratio, it is required to separate the second time-lens (Φ_{f2}) into the eyepiece of the scope ($\Phi_e = -\Phi_{f1} - \Phi_m$) and the single PASTA time-lens ($\Phi_f = \Phi_o$). Therefore, the zoom in ratio can be expressed by:

$$G = -\frac{\Phi_{f1}}{\Phi_e} = \frac{\Phi_{f1}}{\Phi_{f1} + \Phi_m} = \frac{\Phi_{p1}}{\Phi_{p1} + 2\Phi_m} \qquad (3)$$

Dispersive fibers. DCF has much larger dispersion-to-loss ratio than standard SMF-28, which means SMF can provide the same amount of dispersion but with larger insertion loss. For example, the 2-ns/nm output dispersion by DCF introduces 8-dB insertion loss; if replaced by SMF with equal dispersion, the loss will be up to 30 dB. For the alternative configuration of the telescope PASTA, the telephoto lens requires 10 times larger dispersion, and the minimum insertion loss would be 80 dB, almost impossible to compensate. Two erbium-doped fiber amplifiers (EDFAs) were inserted to compensate for the FWM conversion efficiency.

Trigger signal. It is essential to calibrate multi-frames (separation and re-alignment), since all spectral frames are captured as an entire trace from the real-time oscilloscope. There are two approaches for obtaining this trigger signal: (a) directly from the pump pulses, though this can only recover the relative spectral positions; (b) generated by injecting a CW source with known wavelength into the PASTA, which can recover the precise spectral frames. Here, we employed the latter approach.

Noise figure. In general optical amplification or wavelength conversion processes, the increase of the noise power is usually larger than that of the signal, and noise figure is the measure of the degradation of the signal-to-noise ratio: $F_n = SNR_{in}/SNR_{out}$. In most photonic systems, more than one component introduces noise, and it is essential to calculate the cascaded noise figure. The following equation (Friis' formula) is used to calculate the cascaded noise figure:

$$F_n = F_{n1} + \sum_{i=2}^{N} \frac{F_{ni} - 1}{\prod_{j=1}^{i-1} G_j} \qquad (4)$$

where N is the number of stages[31]. As this equation shows, the cascaded noise figure is mostly affected by the noise figure of components closest to the input of the system. In the PASTA system, the signal channel is mainly composed of the EDFAs and the FWM-based wavelength converters. For an ideal EDFA with $n_{sp} = 1$, the noise figure can be expressed as: $F_n = 2 - 1/G$[30]. In the wavelength conversion process, the conversion efficiency η is critical, and the quantum-limited noise figure can be expressed as: $F_n = 2 + 1/\eta$[32]. If this conversion is

accompanied with amplification (G), then the noise figure becomes: $F_n = 2G/(G-1)$[33].

1. Spörlein, S. et al. Ultrafast spectroscopy reveals subnanosecond peptide conformational dynamics and validates molecular dynamics simulation. *PNAS* **99**, 7998–8002 (2002).
2. Evans, C. L. & Xie, X. S. Coherent Anti-Stokes Raman Scattering Microscopy: Chemical Imaging for Biology and Medicine. *Annu. Rev. Anal. Chem.* **1**, 883–909 (2008).
3. Goda, K., Tsia, K. K. & Jalali, B. Serial time-encoded amplified imaging for real-time observation of fast dynamic phenomena. *Nature* **458**, 1145–1149 (2009).
4. Petty, H. R. Spatiotemporal chemical dynamics in living cells: from information trafficking to cell physiology. *Biosystems* **83**, 217–224 (2004).
5. Chou, J., Han, Y. & Jalali, B. Time-wavelength spectroscopy for chemical sensing. *IEEE Photon. Technol. Lett.* **16**, 1140–1142 (2004).
6. Talley, C. E. et al. Surface-Enhanced Raman Scattering from Individual Au Nanoparticles and Nanoparticle Dimer Substrates. *Nano Letters* **5**, 1569–1574 (2005).
7. Shafer, A. B., Megill, L. R. & Droppleman, L. A. Optimization of the Czerny–Turner spectrometer. *J. Opt. Soc. Am.* **54**, 879–887 (1964).
8. Solli, D. R., Chou, J. & Jalali, B. Amplified wavelength-time transformation for real-time spectroscopy. *Nat. Photonics* **2**, 48–51 (2008).
9. Goda, K. & Jalali, B. Dispersive Fourier transformation for fast continuous single-shot measurements. *Nat. Photonics* **7**, 102–112 (2013).
10. Zhang, C., Xu, J., Chui, P. C. & Wong, K. K. Y. Parametric spectro-temporal analyzer (PASTA) for real-time optical spectrum observation. *Sci. Rep.* **3**, 2064; DOI: 10.1038/srep02064 (2013).
11. Zhang, C., Wei, X. & Wong, K. K. Y. Performance of parametric spectro-temporal analyzer (PASTA). *Opt. Express* **21**, 32111–32122 (2013).
12. Okawachi, Y. et al. High-resolution spectroscopy using a frequency magnifier. *Opt. Express* **17**, 5691–5697 (2009).
13. Yokogawa, AQ6370C Optical Spectrum Analyzer, http://tmi.yokogawa.com/files/uploaded/BUAQ6370SR_10EN_010.pdf (June 2011) Date of access: 29/05/2014.
14. Kolner, B. H. Space-Time Duality and the Theory of Temporal Imaging. *IEEE J. Quantum Electron.* **30**, 1951–1963 (1994).
15. Salem, R. et al. High-speed optical sampling using a silicon-chip temporal magnifier. *Opt. Express* **17**, 4324–4329 (2009).
16. Foster, M. A. et al. Ultrafast waveform compression using a time-domain telescope. *Nat. Photonics* **3**, 581–585 (2009).
17. Foster, M. A. et al. Silicon-chip-based ultrafast optical oscilloscope. *Nature* **456**, 81–85 (2008).
18. Lindberg, D. C. A reconsideration of Roger Bacon's theory of pinhole images. *Archive for History of Exact Sciences* **6**, 214–233 (1970).
19. Goda, K., Solli, D. R., Tsia, K. K. & Jalali, B. Theory of amplified dispersive Fourier transformation. *Phys. Rev. A* **80**, 043821 (2009).
20. Nikon, A. F.-S. DX Nikkor 18–300 mm f/3.5–5.6 G, http://imaging.nikon.com/lineup/lens/zoom/normalzoom/af-s_dx_18-300mmf_35-56g_ed_vr/index.htm (June 2012) Date of access: 29/05/2014.
21. Conrady, A. E. *Applied Optics and Optical Design,* Part One (Courier Dover Publications, 2011).
22. Zhang, C., Cheung, K. K. Y., Chui, P. C., Tsia, K. K. & Wong, K. K. Y. Fiber Optical Parametric Amplifier with High-Speed Swept Pump. *IEEE Photon. Technol. Lett.* **23**, 1022–1024 (2011).
23. Zhang, C., Chui, P. C. & Wong, K. K. Y. Comparison of state-of-art phase modulators and parametric mixers in time-lens applications under different repetition rates. *Appl. Opt.* **52**, 8817–8826 (2013).
24. Gu, C., Ilan, B. & Sharping, J. E. Demonstration of nondegenerate spectrum reversal in optical-frequency regime. *Opt. Lett.* **38**, 591–593 (2013).
25. Agrawal, G. P. [Chapter 10 Four-wave mixing] *Nonlinear Fiber Optics* 4th edn [370–374] (Academic Press, 2007).
26. Marhic, M. E. *Fiber Optical Parametric Amplifiers, Oscillators and Related Devices.* (Cambridge University Press, 2007).
27. Mesa Photonics, FROG Scan Users Manual, http://www.mesaphotonics.com/wp-content/themes/Mesaphotonics/images/Frog%20Scan%20Flyer%202011.pdf (April 2011) Date of access: 29/05/2014.
28. Aragon Photonics, BOSA100 & 200 series – Brillouin High Resolution OSA, http://aragonphotonics.com/?page_id=149 (March 2014) Date of access: 29/05/2014.
29. Agilent, 8614xB Series Optical Spectrum Analyzer User's Guide, http://cp.literature.agilent.com/litweb/pdf/86140-90U03.pdf (June 2005) Date of access: 29/05/2014.
30. Turner-Foster, A. C., Foster, M. A., Salem, R., Gaeta, A. L. & Lipson, M. Frequency conversion over two-thirds of an octave in silicon nanowaveguides. *Opt. Express* **18**, 1904–1908 (2010).
31. Agrawal, G. P. [Chapter 7 Loss Management] *Fiber-Optic Communication Systems* 4th edn [318–321] (John Wiley & Sons, Inc., 2010).
32. Hedekvist, P. O. & Andrekson, P. A. "Noise Characteristics of Fiber-Based Optical Phase Conjugators." *IEEE J. Lightwave Technol.* **17**, 74–79 (1999).

33. Kylemark, P., Hedekvist, P. O., Sunnerud, H., Karlsson, M. & Andrekson, P. A. "Noise Characteristics of Fiber Optical Parametric Amplifiers." *IEEE J. Lightwave Technol.* **22**, 409–416 (2004).

Author contributions

The experiment was designed and implemented by C.Z. and X.W., K.W. and C.Z. developed the concept. K.W. and M.M. supervised measurements and analysis. All authors contributed to the preparation of the manuscript.

Additional information